PERGAMON

International Journal of Solids and Structures 40 (2003) 4615–4635

INTERNATIONAL JOURNAL OF SOLIDS and STRUCTURES

www.elsevier.com/locate/ijsolstr

Numerical solutions of two-dimensional anisotropic crack problems

R.K.L. Su [a,*], H.Y. Sun [b]

[a] *Department of Civil Engineering, The University of Hong Kong, Pokfulam Road, Hong Kong, People's Republic of China*
[b] *Department of Civil Engineering, The University of Hong Kong, Pokfulam Road, Hong Kong, People's Republic of China*

Received 14 May 2003; received in revised form 14 May 2003

Abstract

A complete set of series form solutions of stress and displacement functions, including all higher order terms, around the crack tip for anisotropic crack problems have been newly derived by eigenfunction expansion approach. The analytical solutions of displacement functions were classified into four cases with respect to different types of complex parameters and different corresponding physical meanings. By employing these displacement functions as global interpolation functions, fractal two-level finite element method (F2LFEM) was applied to evaluate the stress intensity factors (SIFs) for various kinds of anisotropic crack problems. In the method of F2LFEM, the infinite number of nodal displacements was transformed to a small set of generalized coordinates by fractal transformation technique. New element matrices need not be generated and the singular numerical integration was avoided completely. Numerical examples of the four cases were studied and high accurate results of SIFs were obtained.

Keywords: Eigenfunction expansion; Anisotropic; Crack; Higher order terms; Stress intensity factor; Fractal; Two-level; Global interpolation

1. Introduction

The usefulness of the stress intensity factors (SIFs) in the analysis of the problems of residual strength, fatigue crack growth rate and stress corrosion has resulted in effort being expanded on the determination of SIFs. The use of the SIF in examining crack stability requires an accurate prediction or estimation of the stress field in the vicinity of the crack tip for the given structural geometry, loading and boundary conditions. However, analytical solutions only exist for certain relatively simple cases due to the complicated boundary conditions associated with the governing equations. Over the last decade or so, finite element method (FEM) has been firmly established as a standard procedure for the solution of practical fracture problems. A number of techniques have been suggested for the evaluation of SIF from the finite element

* Corresponding author. Tel.: +85-228592648; fax: +85-225595337.
E-mail address: klsu@hkucc.hku.hk (R.K.L. Su).

0020-7683/03/$ - see front matter © 2003 Elsevier Ltd. All rights reserved.
doi:10.1016/S0020-7683(03)00310-X

results but adequate representation of the crack tip singularity remains a common problem to most of these methods.

Fractal finite elements is originated with Panagiotopoulos (1992, 1993). He adopted the iterated function system to model fractal boundaries and fractal bodies, obtaining asymptotic results for stresses and strains in elastic bodies by classical finite element method. The normal and tangent loads acting on the fractal boundaries were thoroughly investigated and defined using the method of fractal interpolation function. Recently Carpinteri et al. (2001) introduced a new mathematical formulation to handle the mechanical quantities of displacements and total energy of fractal bodies based on fractional calculus. The principle of virtual work for fractal media was rigorously demonstrated and the fractal FEM was introduced by the use of devil's staircase spline functions.

The use of fractal geometry to generate infinite number of finite elements around the crack tips has been adopted by Hu et al. (1998), Song and Wolf (2002) and Leung and Su (1994, 1995b, 1998c). The method proposed by Leung and Su was entitled fractal two-level finite element method (F2LFEM). The advantage of this method is that instead of solving large number of unknowns for conventional finite element meshes, after fractal transformation by the global interpolation functions, only a small set of generalized coordinates remains to be determined. The singularity of the crack tip is modeled by the fractal geometry concepts such that infinitesimal mesh refinement around the crack tip can be achieved. The SIF can be obtained directly from the generalized coordinates without any post-processing technique.

The method of F2LFEM has been successfully applied to solve many kinds of crack problems such as mode I, II, III and mixed-mode 2D cracks (Leung and Su, 1994,1995a,b,1996a,c), cracked classical and Reissner's Plates (Leung and Su, 1996b,d; Su et al., 1998; Su and Leung, 2001a; Su and Sun, 2002), axisymmetric cracks (Leung and Su, 1998c), penny-shaped and circumferential cracks (Leung and Su, 1998b), vibration of cracked beams (Leung and Su, 1998a), together with three-dimensional (3D) cracks (Leung and Su, 1995c; Su and Leung, 2001b). Recently, this method has been found to be able to evaluate the coefficients of the higher order terms of the crack tip asymptotic field (Su et al., 2003). Upon the above review, this method has been proved to be efficient and accurate to evaluate the SIFs for cracks in elastic and isotropic materials. Now this method is extended to tackle elastic anisotropic crack problems, using the newly derived displacement functions around the crack tip (Sun, 2003) as the global interpolation functions.

2. Fractal two-level finite element method

2.1. Introductory formulation of anisotropic elasticity

For a through cracked composite lamina in a state of plane stress, the equations of equilibrium in the absence of body forces are

$$\frac{\partial \sigma_x}{\partial x}+\frac{\partial \tau_{xy}}{\partial y}=0, \quad \frac{\partial \tau_{xy}}{\partial x}+\frac{\partial \sigma_y}{\partial y}=0. \tag{1}$$

The strain–stress relation for a homogeneous anisotropic material is

$$\begin{Bmatrix} \varepsilon_x \\ \varepsilon_y \\ \gamma_{xy} \end{Bmatrix} = \begin{bmatrix} a_{11} & a_{12} & a_{16} \\ a_{12} & a_{22} & a_{26} \\ a_{16} & a_{26} & a_{66} \end{bmatrix} \begin{Bmatrix} \sigma_x \\ \sigma_y \\ \tau_{xy} \end{Bmatrix}. \tag{2}$$

Due to the symmetry of compliance matrix, there are altogether six independent constants. Substituting the stress–strain relation (2) into the following compatibility equation

$$\frac{\partial^2 \varepsilon_x}{\partial y^2} + \frac{\partial^2 \varepsilon_y}{\partial x^2} - \frac{\partial^2 \gamma_{xy}}{\partial x \partial y} = 0 \tag{3}$$

results in

$$\frac{\partial^2}{\partial y^2}(a_{11}\sigma_x + a_{12}\sigma_y + a_{16}\tau_{xy}) + \frac{\partial^2}{\partial x^2}(a_{12}\sigma_x + a_{22}\sigma_y + a_{26}\tau_{xy}) - \frac{\partial^2}{\partial x \partial y}(a_{16}\sigma_x + a_{26}\sigma_y + a_{66}\tau_{xy}) = 0. \tag{4}$$

A stress function, F, is defined as follows such that the equilibrium equations can be satisfied

$$\sigma_x = \frac{\partial^2 F}{\partial y^2}, \quad \sigma_y = \frac{\partial^2 F}{\partial x^2}, \quad \tau_{xy} = -\frac{\partial^2 F}{\partial x \partial y}. \tag{5}$$

Substituting the above stress functions into Eq. (4), the governing equation is obtained

$$a_{22}\frac{\partial^4 F}{\partial x^4} - 2a_{26}\frac{\partial^4 F}{\partial x^3 \partial y} + (2a_{12} + a_{66})\frac{\partial^4 F}{\partial x^2 \partial y^2} - 2a_{16}\frac{\partial^4 F}{\partial x \partial y^3} + a_{11}\frac{\partial^4 F}{\partial y^4} = 0. \tag{6}$$

This equation can also be written in terms of differential operators as

$$D_1 D_2 D_3 D_4 = 0, \tag{7}$$

where

$$D_i = \left(\frac{\partial}{\partial y} - \mu_i \frac{\partial}{\partial x}\right), \quad i = 1, 2, 3, 4$$

and μ_i are the characteristic roots of the characteristic equation

$$a_{11}\mu^4 - 2a_{16}\mu^3 + (2a_{12} + a_{66})\mu^2 - 2a_{26}\mu + a_{22} = 0. \tag{8}$$

It has been proved by Lekhnitskii (1963) that the characteristic Eq. (8) could have either complex, or purely imaginary roots but could not have real roots in the case of any ideal elastic body with real constants $a_{11}, 2a_{12} + a_{66}, a_{22}$ not equal to zero. The general form of the characteristic roots can be denoted as,

$$\begin{aligned} &\mu_1 = \alpha + \mathrm{i}\beta, \quad \mu_2 = \gamma + \mathrm{i}\delta, \\ &\mu_3 = \overline{\mu}_1 = \alpha - \mathrm{i}\beta, \quad \mu_4 = \overline{\mu}_2 = \gamma - \mathrm{i}\delta. \end{aligned} \tag{9}$$

The quantities of μ_1 and μ_2 are called the complex parameters which characterize the degree of anisotropy in the case of plane problems. According to their values it can be judged how much a given body differs from that of the isotropic, for which $\mu_1 = \mu_2$ always equal to i.

The complex parameters got from characteristic Eq. (8) can be grouped into four cases (Sun, 2003). As shown in Fig. 1, Cases I–III correspond to orthotropic cases with the elasticity axes parallel to the coordinate axes, and Case IV corresponds to a general orientation of elasticity axes. For Cases I–III when the terms $a_{16} = a_{26} = 0$ in the compliance matrix, the characteristic Eq. (8) will be the form

$$\mu^4 + 2\left(\frac{E_1}{2G_{12}} - v_{12}\right)\mu^2 + \frac{E_1}{E_2} = 0. \tag{10}$$

Introducing the notations of $A = (E_1/2G_{12}) - v_{12}$ and $B = E_1/E_2$, different type of roots μ_1 and μ_2 can be got based on different relations between A and B as shown in Table 1. These different roots (complex parameters) will lead to different final analytical solutions shown in next section. This is also the main reason why Cases I–III are separated although they have the same physical meanings.

For Case IV when coordinate system and the elasticity axes do not coincide with each other, the characteristic Eq. (8) will be a fourth order equation. To avoid dealing with this complicated equation, it has been shown by Lekhnitskii et al. (1968) that a simple transformation formula shown below can be

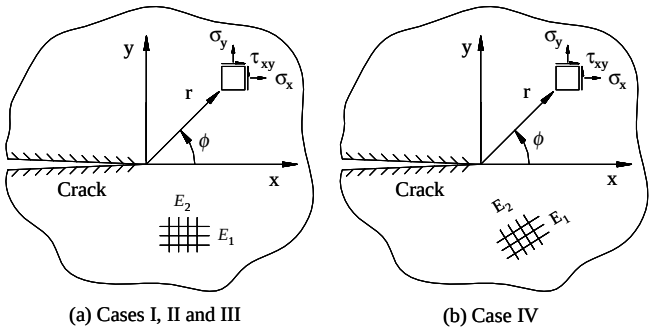

Fig. 1. Classification of anisotropic crack problems concerned.

Table 1
Classification of anisotropic crack problems based on the complex parameters μ

Case	Orientation of elasticity axes	Coefficients of the compliance matrix	The complex parameters
I	Orthotropy and coincident with the coordinate axis, see Fig. 1(a).	$a_{11}, a_{22}, a_{66}, a_{12} \neq 0$, $a_{16} = a_{26} = 0$	$\mu_1 = \mathrm{i}\sqrt{A + \sqrt{A^2 - B}} = \mathrm{i}\beta$, $\mu_2 = \mathrm{i}\sqrt{A - \sqrt{A^2 - B}} = \mathrm{i}\delta$.
II			$\mu_1 = \mathrm{i}\sqrt{\sqrt{B}} = \mathrm{i}\beta$, $\mu_2 = \mu_1$.
III			$\mu_1 = \sqrt{-A \pm \mathrm{i}\sqrt{B - A^2}} = \alpha + \mathrm{i}\beta$, $\mu_2 = -\alpha + \mathrm{i}\beta$.
IV	Orthotropy but not coincident with the coordinate axis, see Fig. 1(b).	$a_{11}, a_{22}, a_{66}, a_{12}, a_{16}, a_{26} \neq 0$	$\mu_1' = \dfrac{\mu_1 \cos\theta - \sin\theta}{\cos\theta + \mu_1 \sin\theta} = \alpha + \mathrm{i}\beta$, $\mu_2' = \dfrac{\mu_2 \cos\theta - \sin\theta}{\cos\theta + \mu_2 \sin\theta} = \gamma + \mathrm{i}\delta$.

Note: $A = E_1/2G_{12} - v_{12}$ and $B = E_1/E_2$.

followed to get the complex parameters in coordinate system $x'oy'$ from those in xoy (see Fig. 2), and the complex parameters μ_1 and μ_2 in xoy can be obtained from Eq. (9).

$$\mu_1' = \frac{\mu_1 \cos\theta - \sin\theta}{\cos\theta + \mu_1 \sin\theta}, \quad \mu_2' = \frac{\mu_2 \cos\theta - \sin\theta}{\cos\theta + \mu_2 \sin\theta}. \tag{11}$$

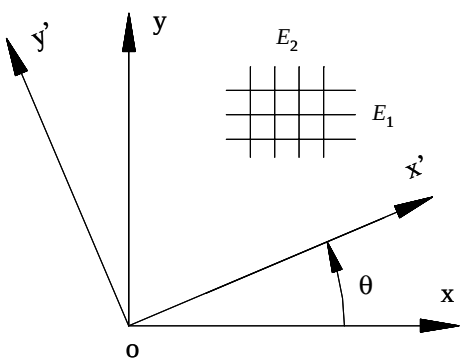

Fig. 2. The complex parameters in two coordinates.

2.2. Global interpolation function

By adopting appropriate form of stress function F (Eq. (5)), adding up the boundary conditions, the analytical solutions of stress and displacement near the crack tip were derived by Sun (2003) using eigenfunction expansion technique. Those series form of displacement functions shown below can serve as global interpolation function in F2LFEM:

(1) Case I:

$$\begin{aligned}
u &= 2\sum_{j=1(\text{odd})}^{\infty}\zeta\left\{b_{1j}\left(-\frac{\delta}{\beta}r_1^{\psi}m_1\cos\psi\theta_1+r_2^{\psi}m_2\cos\psi\theta_2\right)+b_{2j}(r_1^{\psi}m_1\sin\psi\theta_1-r_2^{\psi}m_2\sin\psi\theta_2)\right\}\\
&\quad+2\sum_{j=2(\text{even})}^{\infty}\zeta\left\{b_{1j}(-r_1^{\psi}m_1\cos\psi\theta_1+r_2^{\psi}m_2\cos\psi\theta_2)+b_{2j}\left(r_1^{\psi}\frac{\delta}{\beta}m_1\sin\psi\theta_1-r_2^{\psi}m_2\sin\psi\theta_2\right)\right\},\\
v &= 2\sum_{j=1(\text{odd})}^{\infty}\zeta\left\{b_{1j}\left(-\frac{\delta}{\beta}r_1^{\psi}n_1\sin\psi\theta_1+r_2^{\psi}n_2\sin\psi\theta_2\right)-b_{2j}(r_1^{\psi}n_1\cos\psi\theta_1-r_2^{\psi}n_2\cos\psi\theta_2)\right\}\\
&\quad+\sum_{j=2(\text{even})}^{\infty}\zeta\left\{b_{1j}(-r_1^{\psi}n_1\sin\psi\theta_1+r_2^{\psi}n_2\sin\psi\theta_2)-b_{2j}\left(r_1^{\psi}\frac{\delta}{\beta}n_1\cos\psi\theta_1-r_2^{\psi}n_2\cos\psi\theta_2\right)\right\},
\end{aligned}\tag{12}$$

where β and δ are the imaginary parts of the complex parameters (see Case I in Table 1), $\lambda_j = j/2$ (eigenvalue), $\zeta = \lambda_j + 1$, $\psi = \lambda_j$ ($j = 1, 2, 3, 4$, etc.).

$$m_1 = -a_{11}\beta^2 + a_{12},\quad m_2 = -a_{11}\delta^2 + a_{12},\quad n_1 = -a_{12}\beta + \frac{a_{22}}{\beta},\quad n_2 = -a_{12}\delta + \frac{a_{22}}{\delta},$$

$$r_1 = r\sqrt{\cos^2\phi + \beta^2\sin^2\phi},\quad \theta_1 = \arctan\frac{\beta\sin\phi}{\cos\phi},$$

$$r_2 = r\sqrt{\cos^2\phi + \delta^2\sin^2\phi},\quad \theta_2 = \arctan\frac{\delta\sin\phi}{\cos\phi}$$

and r and ϕ are the polar coordinates shown in Fig. 1(a).

(2) Case II:

$$\begin{aligned}
u &= -2m_1\sum_{j=0}^{\infty}r_1^{j/2}\left\{b_{1j}\left[\left(-\frac{m_2}{m_1}+\frac{j}{2}+(-1)^j\right)\cos\frac{j}{2}\theta_1-\frac{j}{2}\cos\left(\frac{j}{2}-2\right)\theta_1\right]\right.\\
&\quad\left.-b_{2j}\left[\left(-\frac{m_2}{m_1}+\frac{j}{2}-(-1)^j\right)\sin\frac{j}{2}\theta_1-\frac{j}{2}\sin\left(\frac{j}{2}-2\right)\theta_1\right]\right\},\\
v &= 2n_1\sum_{j=0}^{\infty}r_1^{j/2}\left\{b_{1j}\left[\left(\frac{n_2}{n_1}-\frac{j}{2}-(-1)^j\right)\sin\frac{j}{2}\theta_1+\frac{j}{2}\sin\left(\frac{j}{2}-2\right)\theta_1\right]\right.\\
&\quad\left.+b_{2j}\left[\left(\frac{n_2}{n_1}-\frac{j}{2}+(-1)^j\right)\cos\frac{j}{2}\theta_1+\frac{j}{2}\cos\left(\frac{j}{2}-2\right)\theta_1\right]\right\},
\end{aligned}\tag{13}$$

where β is the imaginary part of the complex parameter (see Case II in Table 1),

$$m_1 = -a_{11}\beta^2 + a_{12},\quad m_2 = 3a_{11}\beta^2 + a_{12},\quad n_1 = -a_{12}\beta + \frac{a_{22}}{\beta},\quad n_2 = a_{12}\beta + \frac{3a_{22}}{\beta},$$

$$r_1 = r\sqrt{\cos^2\phi + \beta^2\sin^2\phi}, \quad \theta_1 = \arctan\frac{\beta\sin\phi}{\cos\phi}$$

and r and ϕ are the polar coordinates shown in Fig. 1(a).

(3) Cases III and IV:

$$\begin{aligned} u = 2\sum_{j=1(\text{odd})}^{\infty} a_{1j}\Bigg\{ & r_1^{\psi}\left[\left(\hat{p}_1 + \hat{p}_2\frac{\beta}{\chi}\right)\cos\psi\theta_1 + \left(\hat{p}_1\frac{\beta}{\chi} - \hat{p}_2\right)\sin\psi\theta_1\right] \\ & - r_2^{\psi}\left[\tilde{p}_2\frac{\beta}{\chi}\cos\psi\theta_2 + \tilde{p}_1\frac{\beta}{\chi}\sin\psi\theta_2\right]\Bigg\} + b_{1j}\zeta\Bigg\{ r_1^{\psi}\left(\hat{p}_2\frac{\delta}{\chi}\cos\psi\theta_1 + \hat{p}_1\frac{\delta}{\chi}\sin\psi\theta_1\right) \\ & + r_2^{\psi}\left[\left(\tilde{p}_1 - \tilde{p}_2\frac{\delta}{\chi}\right)\cos\psi\theta_2 - \left(\tilde{p}_2 + \tilde{p}_1\frac{\delta}{\chi}\right)\sin\psi\theta_2\right]\Bigg\} + 2\sum_{j=2(\text{even})}^{\infty} a_{2j}\Bigg\{ r_1^{\psi}\Bigg[\left(\hat{p}_1\frac{\beta}{\chi} - \hat{p}_2\right)\cos\psi\theta_1 \\ & - \left(\hat{p}_1 + \hat{p}_2\frac{\beta}{\chi}\right)\sin\psi\theta_1\Bigg] - r_2^{\psi}\left[\tilde{p}_1\frac{\beta}{\chi}\cos\psi\theta_2 - \tilde{p}_2\frac{\beta}{\chi}\sin\psi\theta_2\right]\Bigg\} + \zeta b_{2j}\Bigg\{ r_1^{\psi}\left[\hat{p}_1\frac{\delta}{\chi}\cos\psi\theta_1 - \hat{p}_2\frac{\delta}{\chi}\sin\psi\theta_1\right] \\ & - r_2^{\psi}\left[\left(\tilde{p}_1\frac{\delta}{\chi} + \tilde{p}_2\right)\cos\psi\theta_2 + \left(\tilde{p}_1 - \tilde{p}_2\frac{\delta}{\chi}\right)\sin\psi\theta_2\right]\Bigg\}. \end{aligned} \tag{14}$$

The v component of the displacement can be obtained by replacing $\hat{p}_k$ by $\hat{q}_k$ and $\tilde{p}_k$ by $\tilde{q}_k$ $(k = 1, 2)$ in the above Eq. (14).Where α, β, γ and δ can be found in Table 1 (Cases III and IV),

$$\lambda_j = j/2, \quad \zeta = \lambda_j + 1, \quad \psi = \lambda_j, \quad \omega = \lambda_j - 1, \quad \chi = \alpha - \gamma \ \ (j = 1, 2, 3, 4, \text{etc.}),$$

$$\hat{p}_1 = a_{11}(\alpha^2 - \beta^2) + a_{12} - a_{16}\alpha, \quad \hat{p}_2 = 2a_{11}\alpha\beta - a_{16}\beta,$$

$$\tilde{p}_1 = a_{11}(\gamma^2 - \delta^2) + a_{12} - a_{16}\gamma, \quad \tilde{p}_2 = 2a_{11}\gamma\delta - a_{16}\delta,$$

$$\hat{q}_1 = a_{12}\alpha + a_{22}\frac{\alpha}{\alpha^2 + \beta^2} - a_{26}, \quad \hat{q}_2 = a_{12}\beta - a_{22}\frac{\beta}{\alpha^2 + \beta^2},$$

$$\tilde{q}_1 = a_{12}\gamma + a_{22}\frac{\gamma}{\gamma^2 + \delta^2} - a_{26}, \quad \tilde{q}_2 = a_{12}\delta - a_{22}\frac{\delta}{\gamma^2 + \delta^2},$$

$$r_1 = r\sqrt{(\cos\phi + \alpha\sin\phi)^2 + \beta^2\sin^2\phi}, \quad \theta_1 = \arctan\frac{\beta\sin\phi}{\cos\phi + \alpha\sin\phi},$$

$$r_2 = r\sqrt{(\cos\phi + \gamma\sin\phi)^2 + \delta^2\sin^2\phi}, \quad \theta_2 = \arctan\frac{\delta\sin\phi}{\cos\phi + \gamma\sin\phi}$$

and r and ϕ are the polar coordinates shown in Fig. 1(b).

In the above Eqs. (12)–(14), the coefficients of a_{1j}, a_{2j}, b_{1j} and b_{2j} are generalized coordinates which are to be determined after loading and boundary conditions are imposed. The relationship between the SIFs and the coefficients can be got by the following definitions:

$$K_{\mathrm{I}} = \lim_{r\to 0}\sqrt{2\pi r}\sigma_y|_{\phi=0}, \quad K_{\mathrm{II}} = \lim_{r\to 0}\sqrt{2\pi r}\tau_{xy}|_{\phi=0}, \tag{15}$$

substituting the corresponding stress components into the above equations, the higher order terms vanish when $r \to 0$ and only the singular term of $1/\sqrt{r}$ remains. Therefore the SIFs are related to the first term of the generalized coordinates (b_{11} and b_{21} or a_{11} and b_{11}) as follows (Sun, 2003),

(1) Case I:

$$K_{\mathrm{I}} = \sqrt{2\pi}\frac{3}{2}b_{11}\left(-\frac{\delta}{\beta}+1\right), \quad K_{\mathrm{II}} = -\sqrt{2\pi}\frac{3}{2}b_{21}(\beta-\delta). \tag{16}$$

(2) Case II:

$$K_{\mathrm{I}} = 2\sqrt{2\pi}b_{11}, \quad K_{\mathrm{II}} = -2\beta\sqrt{2\pi}b_{21}. \tag{17}$$

(3) Cases III and IV:

$$K_{\mathrm{I}} = \sqrt{2\pi}\left(a_{11}+\frac{3}{2}b_{11}\right), \quad K_{\mathrm{II}} = -\sqrt{2\pi}\left[a_{11}\left(\alpha+\frac{\beta^2-\beta\delta}{\alpha-\gamma}\right)+\frac{3}{2}b_{11}\left(\gamma+\frac{\beta\delta-\delta^2}{\alpha-\gamma}\right)\right]. \tag{18}$$

2.3. Formulation of F2LFEM

In the formulation of F2LFEM, the cracked elastic body is divided into the singular region Ψ and the regular regions Ω by the boundary Γ_0 as shown in Fig. 3. In the regular region, the conventional finite elements are adopted and the nodal displacements serve as unknowns. Conventional FEMs suggest the following local (first level) interpolation for the element displacements $\mathbf{u}(\mathbf{x})$,

$$\mathbf{u} = \mathbf{N}\mathbf{d}, \tag{19}$$

where $\mathbf{N} = \mathbf{N}(\xi,\eta)$ is the shape function matrix in terms of the natural coordinates (ξ,η), and $\mathbf{d}$ is the nodal displacement vector.

Within the singular region, an infinite set $\{\Gamma_1,\Gamma_2,\Gamma_3,\ldots\}$ of curves similar to the shape of Γ_0 with proportionality constants $\bar{\xi}^1,\bar{\xi}^2,\bar{\xi}^3,\ldots(0<\bar{\xi}<1)$ are generated. Let the displacements of the master nodes on the boundary Γ_0 be $\mathbf{d}_{\mathrm{m}}$ and those of the slave nodes within the boundary Γ_0 be $\mathbf{d}_{\mathrm{s}}$. The grading of mesh inside the singular region can be controlled by the proportionality constant $\bar{\xi}<1$. Higher values of $\bar{\xi}$ will produce finer grade of mesh and vice versa.

It has been shown (Sun, 2003) that displacements near the crack tip do not vary arbitrarily but follow certain displacement patterns which automatically satisfy the boundary conditions at the crack surface. These displacement patterns serve as good global (second level) interpolation functions for F2LFEM to interpolate the nodal displacements near the crack tip, as follows,

$$\mathbf{d}_{\mathrm{s}}(\mathbf{r},\theta) = \mathbf{T}(\mathbf{r},\theta)\mathbf{a} \tag{20}$$

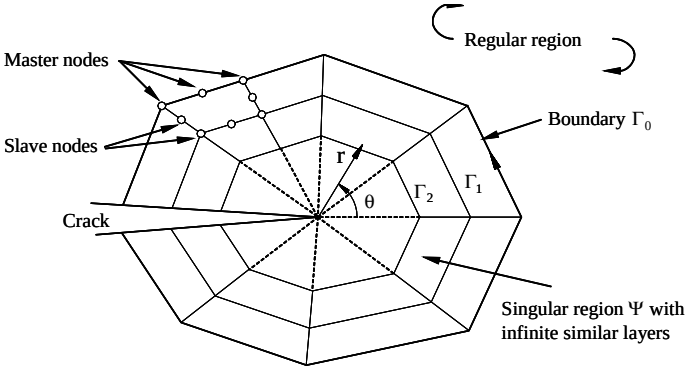

Fig. 3. Regular and singular regions and construction of fractal mesh.

in which $\mathbf{T} = \mathbf{T}(\mathbf{r}, \theta)$ is a transformation matrix and $\mathbf{a}$ is the unknown generalized coordinate vector which is independent of the polar coordinates.

According to the conservation of strain energy, after transformation, the global finite element stiffness equation (Leung and Su, 1994) can be written as

$$\mathbf{K}_r \mathbf{d}_r = \mathbf{Q}_r, \tag{21}$$

$$\overline{\mathbf{K}}_\mathrm{s} \bar{\mathbf{d}}_\mathrm{s} = \overline{\mathbf{Q}}_\mathrm{s}, \tag{22}$$

where

$$\overline{\mathbf{K}}_\mathrm{s} = \begin{bmatrix} \mathbf{K}_{\mathrm{mm}} & \mathbf{K}_{\mathrm{ms}}\mathbf{T} \\ \mathbf{T}^\mathrm{T}\mathbf{K}_{\mathrm{sm}} & \mathbf{T}^\mathrm{T}\mathbf{K}_{\mathrm{ss}}\mathbf{T} \end{bmatrix}, \quad \overline{\mathbf{Q}}_\mathrm{s} = \begin{Bmatrix} \mathbf{Q}_\mathrm{m} \\ \mathbf{T}^\mathrm{T}\mathbf{Q}_\mathrm{s} \end{Bmatrix} \quad \text{and} \quad \bar{\mathbf{d}}_\mathrm{s} = \begin{Bmatrix} \mathbf{d}_\mathrm{m} \\ \mathbf{a} \end{Bmatrix}. \tag{23}$$

2.4. Fractal transformation

To carry out the transformation, the first layer stiffness matrix $\mathbf{K}^\mathrm{f}$ for the first layer of mesh (Fig. 3) is first partitioned with respect to s and m:

$$\mathbf{K}^\mathrm{f}\mathbf{d} = \begin{bmatrix} \mathbf{K}^\mathrm{f}_{\mathrm{ss}} & \mathbf{K}^\mathrm{f}_{\mathrm{sm}} \\ \mathbf{K}^\mathrm{f}_{\mathrm{ms}} & \mathbf{K}^\mathrm{f}_{\mathrm{mm}} \end{bmatrix} \begin{Bmatrix} \mathbf{d}_\mathrm{s} \\ \mathbf{d}_\mathrm{m} \end{Bmatrix}. \tag{24}$$

The displacements at the slaves can be replaced by the global (second level) interpolation function as follows,

$$\begin{Bmatrix} \mathbf{d}_\mathrm{s} \\ \mathbf{d}_\mathrm{m} \end{Bmatrix} = \begin{bmatrix} \mathbf{T}^\mathrm{f}_\mathrm{s} & \mathbf{0} \\ \mathbf{0} & \mathbf{I} \end{bmatrix} \begin{Bmatrix} \mathbf{a} \\ \mathbf{d}_\mathrm{m} \end{Bmatrix}, \tag{25}$$

where the transformation matrix $\mathbf{T}^\mathrm{f}_\mathrm{s}$ can be evaluated by using Eqs. (12)–(14) and $\mathbf{a}$ is the generalized coordinate vector. After transformation, one has,

$$\overline{\mathbf{K}}^\mathrm{f}_\mathrm{s} \begin{Bmatrix} \mathbf{a} \\ \mathbf{d}_\mathrm{m} \end{Bmatrix} = \begin{bmatrix} \mathbf{T}^{\mathrm{f}^\mathrm{T}}_\mathrm{s} \mathbf{K}^\mathrm{f}_{\mathrm{ss}} \mathbf{T}^\mathrm{f}_\mathrm{s} & \mathbf{T}^{\mathrm{f}^\mathrm{T}}_\mathrm{s} \mathbf{K}^\mathrm{f}_{\mathrm{sm}} \\ \mathbf{K}^\mathrm{f}_{\mathrm{ms}} \mathbf{T}^\mathrm{f}_\mathrm{s} & \mathbf{K}^\mathrm{f}_{\mathrm{mm}} \end{bmatrix} \begin{Bmatrix} \mathbf{a} \\ \mathbf{d}_\mathrm{m} \end{Bmatrix}. \tag{26}$$

Furthermore, considering the matrix transformation of the kth inner layer of the element stiffness matrix and the assembly of inner layer of meshes from the second layer to infinite layer, the generalized stiffness matrix $\overline{\mathbf{K}}^i$ is written as

$$\overline{\mathbf{K}}^i \mathbf{a} = \left[\sum_{k=2}^{\infty} \mathbf{T}^{k^\mathrm{T}} \mathbf{K}^k \mathbf{T}^k \right] \mathbf{a}, \tag{27}$$

where $\mathbf{K}^k$ is the stiffness of the kth layer which had been proved to be equal to the stiffness matrix of the first layer (Leung and Su, 1994) and $\mathbf{T}^k$ is the transformation matrix of the kth layer of mesh. Since $\mathbf{T}^k$ is a power series of r, it can be related to the transformation matrix of the first layer $\mathbf{T}^\mathrm{f}$ by

$$\mathbf{T}^k = \mathbf{T}^\mathrm{f} \mathrm{Diag}[\alpha_j], \tag{28}$$

where $\alpha_j = \alpha_j(\bar{\xi}, k)$ is a scaling function for the transformation matrices. By comparing the transformation matrices $\mathbf{T}^k$ and $\mathbf{T}^\mathrm{f}$, it had been shown that $\alpha_j(1/2, k) = 1/2^{j(k-1)}$ when $\bar{\xi} = 1/2$. Putting Eq. (28) into Eq. (27), one has,

$$\overline{\mathbf{K}}^i \mathbf{a} = \left[\sum_{k=2}^{\infty} \mathrm{Diag}[\alpha_i]^\mathrm{T} \mathbf{T}^{\mathrm{f}^\mathrm{T}} \mathbf{K}^\mathrm{f} \mathbf{T}^\mathrm{f} \mathrm{Diag}[\alpha_j] \right] \mathbf{a}. \tag{29}$$

Eq. (29) is a geometrical series, it can be further simplified as

$$\overline{\mathbf{K}}^{i}\mathbf{a} = \begin{bmatrix} & \vdots & \\ \cdots & \overline{\alpha}_{ij}\bar{k}^{\mathrm{f}}_{ij} & \cdots \\ & \vdots & \end{bmatrix}\mathbf{a}, \tag{30}$$

where

$$\overline{\alpha}_{ij} = \sum_{k=2}^{\infty}\alpha_i\alpha_j = \frac{1}{2^{(i+j)}-1}, \tag{31}$$

where $\bar{k}^{\mathrm{f}}_{ij}$ is the ijth entry in matrix $\mathbf{T}^{\mathrm{f}^{\mathrm{T}}}\mathbf{K}^{\mathrm{f}}\mathbf{T}^{\mathrm{f}}$, and $\overline{\alpha}_{ij} = \overline{\alpha}_{ij}(\bar{\xi})$ is a scaling function for the entry. Eq. (30) implies that the transformation and assembly of all the inner layer elements can be accomplished effectively by modifying the generalized stiffness matrix of the first layer using the scaling function $\overline{\alpha}_{ij}$. The complete generalized stiffness matrix for the singular region can be calculated by adding up Eqs. (26) and (30) of the first layer and the inner layers of stiffness matrices, respectively.

3. Numerical examples for Case I crack problems

3.1. Rectangular plates with a central crack under tension

The problems considered are shown in Fig. 4. A rectangular sheet with a central crack of $2a$ is under tensile stress of σ. Bowie and Freese (1972) have successfully presented extensive data on this kind of problems for several different geometries and materials. The SIFs presented by Bowie and Freese have not related to practical material properties, only the value of complex parameters μ_1 and μ_2 rather than the explicit material constants were given. It is therefore considered sufficient to fix β as unity and vary the parameter of δ to find how much the degree of anisotropy can affect the SIFs. According to the relations of two complex parameters (Case I in Table 1), one has

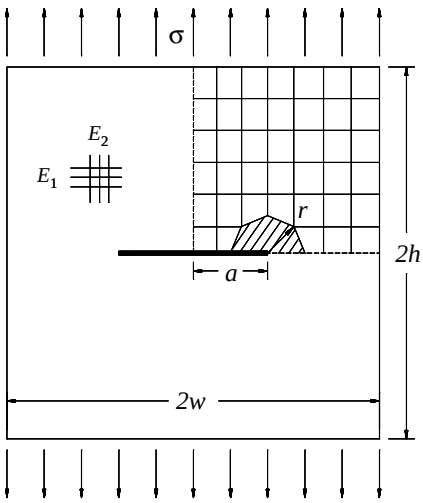

Fig. 4. Single central crack subjected to tension (Hatched area represents the singular region).

$$\beta\delta = \sqrt{E_1/E_2}, \quad \beta + \delta = \sqrt{2}\{\sqrt{(E_1/E_2)} + E_1/2G_{12} - v_{12}\}^{1/2}. \tag{32}$$

Putting $\beta = 1$ into the above equations, one has

$$\delta^2 = E_1/E_2, \quad 1 + \delta = \sqrt{2}\{\sqrt{(E_1/E_2)} + E_1/2G_{12} - v_{12}\}^{1/2}. \tag{33}$$

In the present study, Young's modulus E_1 is fixed as 30 units and v_{12} as 0.3, E_2 and G_{12} are varied to attain the variation of δ^2 as shown in Table 2.

The mesh for F2LFEM analysis is shown in Fig. 4. Due to symmetry of this problem, only one-quarter of the plate needs to be modeled. Three types of height to width ratio ($h/w = 1.0$, 1.5, 2.0) are investigated and each type contains different values of δ^2 and different crack length to specimen width ratio a/w. The dimensionless SIFs got from F2LFEM are tabulated in Tables 3–5 for $h/w = 1.0$, 1.5 and 2.0 respectively. The results are compared with those from Bowie and Freese (1972) in Figs. 5–7. The errors are found to be less than 3.0%.

3.2. Infinite strip with internal crack under tension, pure bending

Infinite orthotropic strip with internal crack subjected to uniform tension and pure bending as shown in Fig. 8 are studied by F2LFEM. The crack varies its position and length by different value of ratios a/h and b/h. For pure bending load case (Fig. 8(b)), the normalizing maximum stress at the edges of the strip is $\sigma = 6M/h^2$. The material properties under consideration are:

Table 2
Material constants and complex parameters for cracked rectangular plate (Case I)

	δ^2	E_1 (Psi $\times 10^6$)	E_2 (Psi $\times 10^6$)	v_{12}	G_{12} (Psi $\times 10^6$)
$\beta = 1$	0.1	30.0	300.0	0.3	17.647
	0.3	30.0	100.0	0.3	15.789
	0.5	30.0	60.0	0.3	14.286
	0.7	30.0	42.857	0.3	13.043
	0.9	30.0	33.333	0.3	12.000
	1.0	30.0	30.0	0.3	11.538
	1.1	30.0	27.273	0.3	11.111
	1.5	30.0	20.0	0.3	9.677
	2.5	30.0	12.0	0.3	7.317
	3.5	30.0	8.571	0.3	5.882
	4.5	30.0	6.667	0.3	4.918

Table 3
SIFs for central crack tension from F2LFEM, $h/w = 1.0$

δ^2	a/w							
	0.1	0.2	0.3	0.4	0.5	0.6	0.7	0.8
0.1	1.035	1.148	1.320	1.540	1.816	2.169	2.606	3.112
0.3	1.027	1.096	1.212	1.369	1.566	1.800	2.076	2.417
0.5	1.020	1.076	1.169	1.297	1.454	1.642	1.874	2.196
0.7	1.016	1.065	1.145	1.254	1.390	1.555	1.769	2.088
0.9	1.014	1.057	1.128	1.226	1.348	1.500	1.704	2.023
1.0	1.013	1.054	1.122	1.215	1.333	1.480	1.681	1.999
1.1	1.012	1.052	1.117	1.206	1.319	1.462	1.661	1.980
1.5	1.009	1.044	1.101	1.179	1.281	1.414	1.606	1.925
2.5	1.006	1.035	1.081	1.146	1.235	1.357	1.543	1.862
3.5	1.004	1.030	1.072	1.131	1.214	1.332	1.514	1.833
4.5	1.003	1.028	1.066	1.123	1.203	1.318	1.498	1.815

Table 4
SIFs for central crack tension from F2LFEM, $h/w = 1.5$

δ^2	a/w							
	0.1	0.2	0.3	0.4	0.5	0.6	0.7	0.8
0.1	1.031	1.070	1.165	1.291	1.442	1.618	1.820	2.123
0.2	1.022	1.056	1.126	1.219	1.335	1.478	1.670	1.983
0.3	1.015	1.046	1.103	1.181	1.282	1.413	1.604	1.924
0.5	1.009	1.036	1.081	1.147	1.235	1.358	1.548	1.875
0.7	1.006	1.031	1.072	1.132	1.215	1.336	1.525	1.854
0.9	1.004	1.028	1.067	1.124	1.205	1.324	1.513	1.843
1.0	1.003	1.028	1.065	1.121	1.202	1.320	1.509	1.839
1.1	1.003	1.027	1.064	1.119	1.199	1.317	1.505	1.835

Table 5
SIFs for central crack tension from F2LFEM, $h/w = 2.0$

δ^2	a/w							
	0.1	0.2	0.3	0.4	0.5	0.6	0.7	0.8
0.1	1.022	1.036	1.093	1.171	1.268	1.391	1.558	1.864
0.2	1.016	1.033	1.076	1.137	1.221	1.338	1.519	1.843
0.3	1.010	1.029	1.066	1.122	1.202	1.318	1.505	1.834
0.4	1.008	1.026	1.062	1.116	1.195	1.311	1.499	1.831
0.5	1.006	1.025	1.060	1.113	1.191	1.308	1.497	1.829

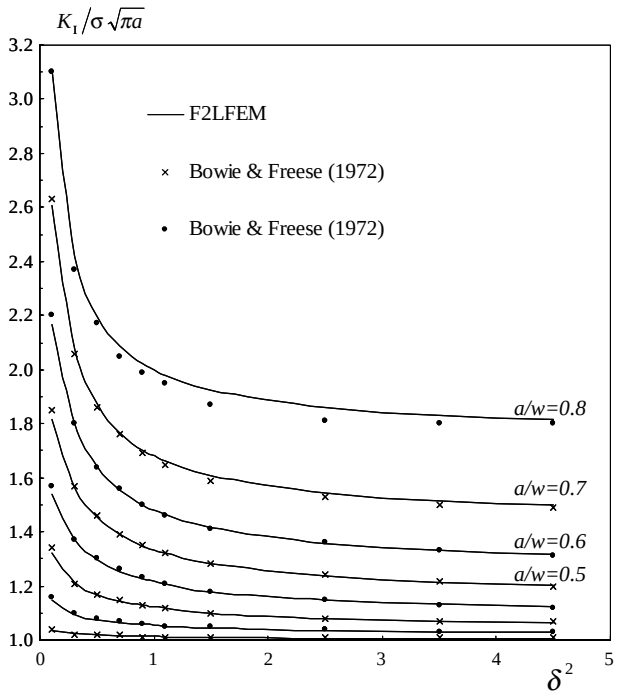

Fig. 5. Comparison of SIFs for cracked rectangular plate, $h/w = 1.0$.

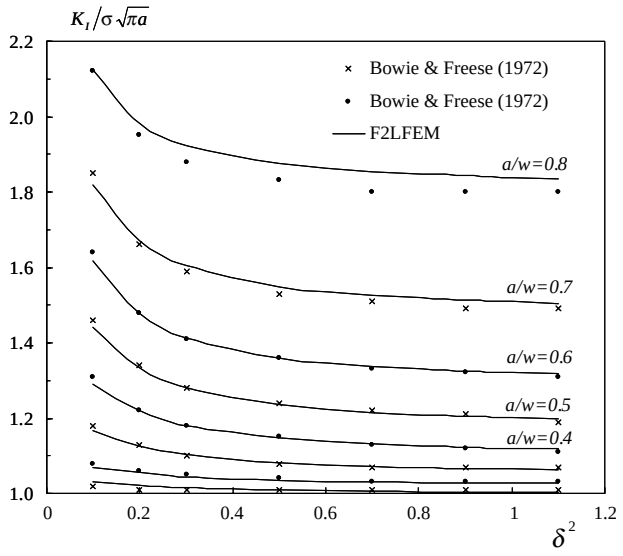

Fig. 6. Comparison of SIFs for cracked rectangular plate, $h/w = 1.5$.

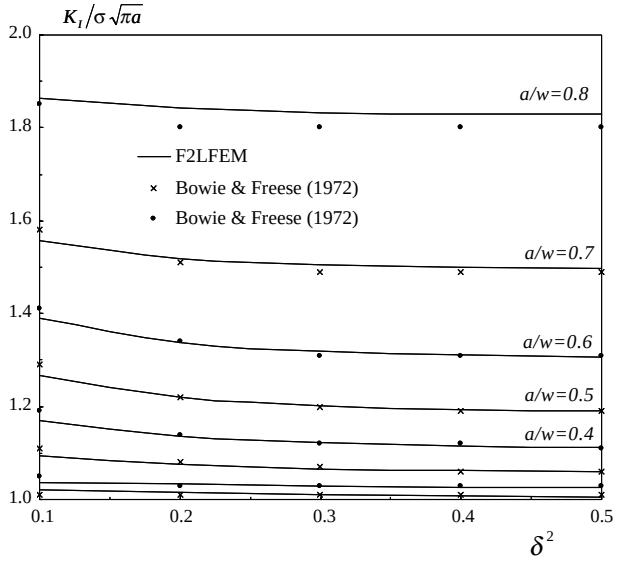

Fig. 7. Comparison of SIFs for cracked rectangular plate, $h/w = 2.0$.

$$E_1 = 170.65 \text{ GPa}, \quad E_2 = 55.16 \text{ GPa}, \quad v_{12} = 0.1114, \quad v_{21} = 0.036.$$

The dimensionless SIFs got from F2LFEM solutions are compared with those from Kaya and Erdogan (1980) for each type of load case and for different kinds of crack geometries. For convenience, the result comparison for $a/h = 0.1$ and 0.2 is tabulated together in Table 6, and the comparison for $a/h = 0.3$ and 0.4 is shown in Table 7. From these two tables, the errors are found to be less than 1.0% generally. It should

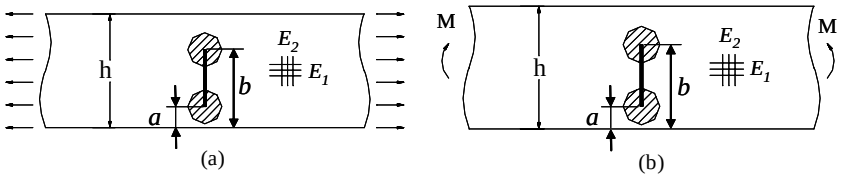

Fig. 8. Infinite strip with internal crack subjected to various loading. (a) Uniform tension, (b) pure bending.

Table 6
SIFs comparison for an internal crack of length $2L$ in an orthotropic strip under tension

b/h	Tension ($a/h = 0.1$)		Pure bending ($a/h = 0.1$)		Tension ($a/h = 0.2$)		Pure bending ($a/h = 0.2$)	
	$K_I(a)/\sigma\sqrt{\pi L}$	$K_I(b)/\sigma\sqrt{\pi L}$	$K_I(a)/\sigma\sqrt{\pi L}$	$K_I(b)/\sigma\sqrt{\pi L}$	$K_I(a)/\sigma\sqrt{\pi L}$	$K_I(b)/\sigma\sqrt{\pi L}$	$K_I(a)/\sigma\sqrt{\pi L}$	$K_I(b)/\sigma\sqrt{\pi L}$
From F2LFEM								
0.2	1.0455	1.0367	0.7823	0.6754				
0.3	1.1213	1.0807	0.7739	0.5495	1.0224	1.0199	0.5616	0.4596
0.4	1.2155	1.1227	0.7630	0.4136	1.0537	1.0400	0.5216	0.3166
0.5	1.3138	1.1555	0.7387	0.2661	1.0947	1.0623	0.4802	0.1694
0.6	1.4057	1.1817	0.6979	0.1090	1.1379	1.0874	0.4326	0.0178
0.7	1.4854	1.2174	0.6419	−0.0564	1.1814	1.1293	0.3780	−0.1400
0.8	1.5538	1.3079	0.5738	−0.2386	1.2301	1.2301	0.3160	−0.3160
0.9	1.6267	1.6267	0.4941	−0.4941	1.3079	1.5538	0.2386	−0.5738
From Kaya and Erdogan (1980)								
0.2	1.0385	1.0296	0.7771	0.6708				
0.3	1.1172	1.0758	0.7717	0.5462	1.0154	1.0129	0.5577	0.4565
0.4	1.2122	1.1183	0.7614	0.4114	1.0494	1.0355	0.5202	0.3145
0.5	1.3106	1.1512	0.7373	0.2647	1.0909	1.0584	0.4791	0.1682
0.6	1.4027	1.1775	0.6967	0.1083	1.1342	1.0836	0.4316	0.0173
0.7	1.4826	1.2133	0.6406	−0.0565	1.1778	1.1255	0.3771	−0.1399
0.8	1.5510	1.304	0.5727	−0.238	1.2264	1.2264	0.3152	−0.3152
0.9	1.6241	1.6241	0.4929	−0.4929	1.3040	1.5510	0.2380	−0.5727
Corresponding errors (%)								
0.2	0.68	0.69	0.67	0.69				
0.3	0.37	0.46	0.28	0.60	0.69	0.69	0.70	0.68
0.4	0.28	0.39	0.21	0.53	0.41	0.43	0.27	0.66
0.5	0.24	0.37	0.19	0.54	0.35	0.37	0.23	0.70
0.6	0.21	0.36	0.18	0.69	0.33	0.35	0.23	2.85
0.7	0.19	0.34	0.20	−0.15	0.31	0.34	0.24	0.08
0.8	0.18	0.30	0.20	0.27	0.30	0.30	0.24	0.24
0.9	0.16	0.16	0.24	0.24	0.30	0.18	0.27	0.20

$L = (b - a)/2$, $a/h = 0.1$ and 0.2.

be noted that the negative SIFs given in Tables 6 and 7 are meaningful only if the results are used in superposition with other results in such a way that the combined SIFs are positive.

4. Numerical examples for Case II crack problems

Although Case II crack problems have not been studied before, the analytical solution of Eq. (13) can be verified by comparing Case II (Eq. (13)) with Case I (Eq. (12)) problems. For Case I crack problems when

Table 7
SIFs comparison for an internal crack of length $2L$ in an orthotropic strip under tension

b/h	Tension ($a/h = 0.3$)		Pure bending ($a/h = 0.3$)		Tension ($a/h = 0.4$)		Pure bending ($a/h = 0.4$)	
	$K_I(a)/\sigma\sqrt{\pi L}$	$K_I(b)/\sigma\sqrt{\pi L}$	$K_I(a)/\sigma\sqrt{\pi L}$	$K_I(b)/\sigma\sqrt{\pi L}$	$K_I(a)/\sigma\sqrt{\pi L}$	$K_I(b)/\sigma\sqrt{\pi L}$	$K_I(a)/\sigma\sqrt{\pi L}$	$K_I(b)/\sigma\sqrt{\pi L}$
From F2LFEM								
0.4	1.0148	1.0138	0.3548	0.2538				
0.5	1.0303	1.0251	0.3059	0.1054	1.0118	1.0116	0.1515	0.0508
0.6	1.0540	1.0451	0.2561	−0.0455	1.0224	1.0224	0.0997	−0.0997
0.7	1.0848	1.0848	0.2020	−0.2020	1.0451	1.0540	0.0455	−0.2561
0.8	1.1293	1.1814	0.1400	−0.3780	1.0874	1.1379	−0.0178	−0.4326
0.9	1.2174	1.4854	0.0564	−0.6419	1.1817	1.4057	−0.1090	−0.6979
From Kaya and Erdogan (1980)								
0.4	1.0079	1.0068	0.3524	0.2521				
0.5	1.0261	1.0208	0.3054	0.1042	1.0049	1.0046	0.1505	0.0505
0.6	1.0504	1.0415	0.2558	−0.0459	1.0182	1.0182	0.1001	−0.1001
0.7	1.0811	1.0811	0.2017	−0.2017	1.0415	1.0504	0.0459	−0.2558
0.8	1.1255	1.1778	0.1399	−0.3771	1.0836	1.1342	−0.0173	−0.4316
0.9	1.2133	1.4826	0.0565	−0.6406	1.1775	1.4027	−0.1083	−0.6966
Corresponding errors (%)								
0.4	0.69	0.69	0.69	0.68				
0.5	0.41	0.42	0.16	1.20	0.69	0.69	0.68	0.64
0.6	0.35	0.35	0.13	−0.84	0.41	0.41	−0.41	−0.41
0.7	0.34	0.34	0.14	0.14	0.35	0.35	−0.84	0.13
0.8	0.34	0.31	0.08	0.24	0.35	0.33	2.85	0.23
0.9	0.34	0.19	−0.15	0.20	0.36	0.21	0.69	0.19

$L = (b - a)/2$, $a/h = 0.3$ and 0.4.

the complex parameters are $\mu_1 = i\beta$ and $\mu_2 = i\delta$, by setting δ close to β, the result of SIF could be approaching that of Case II crack problems. This provides a way to verify the present analytical solutions.

The example considered is a square plate ($h/w = 1.0$) with single central crack of $a/w = 0.5$ as shown in Fig. 4. The verification study is tabulated in Table 8, E_1 and E_2 are set to be 30 and 300 units, v_{12} is set to be 0.3, the shear modulus of G_{12} is varied to approach the Case II crack problems in which the equation of $(E_1/2G_{12} - v_{12})^2 - E_1/E_2 = 0$ can be satisfied. The corresponding SIFs for each types of material are shown in the last column. It can be seen that very good agreement has been obtained when Case I solutions approaching that of Case II which is directly calculated by the new approach derived in the last section.

Table 8
SIFs comparison for Case I approaching and Case II calculation

	E_1	E_2	v_{12}	G_{12}	β	δ	K_I
Case I	30	300	0.3	20	0.87759	0.36034	7.1997
	30	300	0.3	21	0.82579	0.3829	7.2014
	30	300	0.3	22	0.77188	0.40969	7.2038
	30	300	0.3	23	0.71217	0.44404	7.2068
	30	300	0.3	24	0.63246	0.50000	7.2103
	30	300	0.3	24.3	0.58579	0.53983	7.2114
Case II	30	300	0.3	24.34165	0.56236	0.56232	7.2116

5. Numerical examples for Case III crack problems

Examples of internal and edge cracks in a long orthotropic strip considered by Delale and Erdogan (1977) is studied by F2LFEM. As shown in Fig. 9, for each type of problems, only one-quarter of the whole plate needs to be modeled. The hatched areas in the figure represent the singular regions in which fractal meshes are generated by F2LFEM. The material considered is a kind of boron–epoxy composite which possesses the following properties:

$$E_1 = 3.1 \times 10^6 \text{ psi } (21.37 \text{ GPa}), \quad E_2 = 9.7 \times 10^6 \text{ psi } (66.88 \text{ GPa}),$$
$$G_{12} = 2.6 \times 10^6 \text{ psi } (17.93 \text{ GPa}), \quad v_{12} = 0.2.$$

The complex parameters for this kind of orthotropic material are:

$$\mu_1 = 0.29098 + 0.69325\text{i}, \quad \mu_2 = -0.29098 + 0.69325\text{i}.$$

The results from F2LFEM and Delale and Erdogan (1977) are tabulated together in Tables 9 and 10. The percentage of error is generally less than 1.0%.

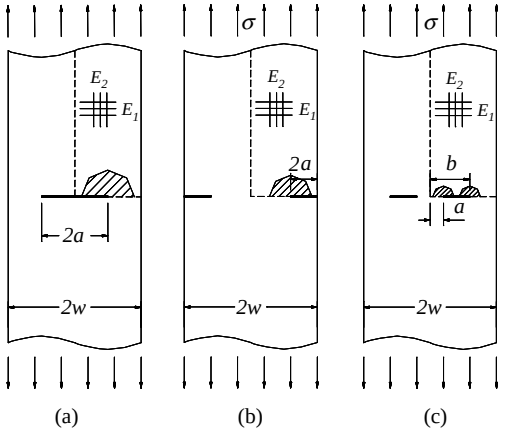

Fig. 9. Infinite strip with central and edge cracks. (a) Infinite strip with an internal crack. (b) Infinite strip with symmetric edge cracks. (c) Infinite strip with symmetric collinear cracks.

Table 9
SIF $K_I/\sigma\sqrt{\pi a}$ for (a) single internal and (b) double edge cracks

a/w	(a) Single internal crack			$2a/w$	(b) Symmetric edge cracks		
	Delale and Erdogan (1977)	F2LFEM	Error (%)		Delale and Erdogan (1977)	F2LFEM	Error (%)
0.1	1.0064	1.0062	−0.02	0.1	1.593	1.599	0.36
0.2	1.0261	1.0258	−0.03	0.2	1.587	1.591	0.26
0.3	1.0611	1.0610	−0.01	0.3	1.590	1.594	0.28
0.4	1.1155	1.1155	0.00	0.4	1.613	1.616	0.19
0.5	1.1966	1.1966	0.00	0.5	1.661	1.665	0.27
0.6	1.3183	1.3184	0.01	0.6	1.750	1.757	0.38
0.7	1.5099	1.5176	0.51	0.7	1.912	1.929	0.89
0.8	1.8471	1.8626	0.84	0.8	2.220	2.250	1.36
0.9	2.6278	2.6298	0.08	0.9	2.982	3.194	7.11

Table 10
SIFs $K_I(a)/\sigma\sqrt{\pi L}$ and $K_I(b)/\sigma\sqrt{\pi L}$ for (c) symmetric collinear cracks of length $2L$ in an orthotropic trip, $2L = b - a$

a/w	b/w	$K_I(a)/\sigma\sqrt{\pi L}$			$K_I(b)/\sigma\sqrt{\pi L}$		
		Delale and Erdogan (1977)	F2LFEM	Error (%)	Delale and Erdogan (1977)	F2LFEM	Error (%)
0.1	0.5	1.179	1.181	0.14	1.117	1.120	0.28
0.2	0.6	1.111	1.117	0.50	1.096	1.101	0.50
0.4	0.8	1.099	1.105	0.50	1.127	1.132	0.45
0.5	0.9	1.132	1.134	0.21	1.231	1.233	0.14
0.1	0.9	1.689	1.691	0.13	1.705	1.707	0.10
0.5	0.95	1.200	1.201	0.09	1.461	1.460	−0.09

6. Numerical examples for Case IV problems

It is well known that cracks usually occur parallel to the fibre direction in composite laminates. The numerical examples of this case where cracks are not parallel to the fibre directions are mainly used for testing the general anisotropic formulation.

6.1. Single edge cracked plate with rotating material axes

As shown in Fig. 10, an example of an edge cracked rectangular plate with one edge fixed under shear is studied. Two kinds of materials shown in Fig. 10 are considered which represents two kinds of graphite–epoxy composite. The modes I and II SIFs are calculated in terms of different orientation of material axes θ. For material 1, the results from F2LFEM solutions are compared with those from Song and Wolf (2002) and Tan and Gao (1992) in Table 11. The errors are found to be less than 1.0%.

The problems shown in Fig. 10 have also been studied by Chu and Hong (1990) for material 2. Their results are compared with those determined from F2LFEM in Table 12. Slightly higher discrepancies are found for mode II SIFs, especially when the value of $K_{II}/\tau\sqrt{\pi a}$ is close to zero. This phenomenon is acceptable since larger numerical error appears when the SIF goes to a very small value.

Chu and Hong (1990) have also studied the problems of single edge-cracked plate under tension with rotating material axes for material 2 and presented their results in graphical form. F2LFEM is used to recalculate the SIFs for this problem and the results from F2LFEM are shown in Table 12 and comparison is shown in Fig. 11.

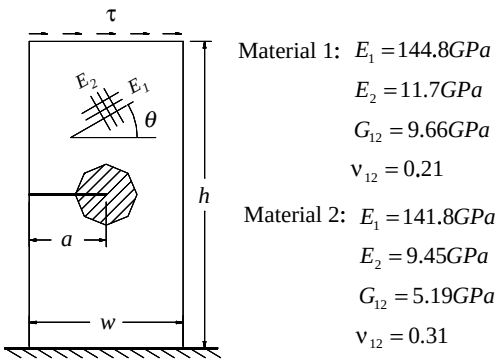

Fig. 10. Single edge cracked plate under shear ($a/w = 0.5$, $h/w = 2.0$).

Table 11
SIFs for single edged-cracked plate under shear (material 1)

θ	F2LFEM		Song and Wolf (2002)		Tan and Gao (1992)		Difference with Song and Wolf (%)	
	$K_I/\tau\sqrt{\pi a}$	$K_{II}/\tau\sqrt{\pi a}$	$K_I/\tau\sqrt{\pi a}$	$K_{II}/\tau\sqrt{\pi a}$	$K_I/\tau\sqrt{\pi a}$	$K_{II}/\tau\sqrt{\pi a}$	Mode I	Mode II
0°	8.801	1.339	8.821	1.341	8.789	1.458	−0.23	−0.17
30°	9.833	5.012	9.852	5.066	9.924	5.122	−0.19	−1.06
60°	9.622	3.395	9.645	3.407	9.697	3.405	−0.23	−0.36
90°	8.835	1.030	8.871	1.029	8.89	1.044	−0.40	0.12
120°	11.231	−1.280						
150°	10.348	−2.472						
160°	9.669	−1.888						
170°	9.061	−0.591						
180°	8.801	1.339						

Table 12
SIFs for single edged-cracked plate under shear and tension (material 2)

θ	Single edge-cracked plate under shear						Tension (Fig. 11)	
	F2LFEM		Chu and Hong (1990)		Error (%)		F2LFEM	
	$K_I/\tau\sqrt{\pi a}$	$K_{II}/\tau\sqrt{\pi a}$	$K_I/\tau\sqrt{\pi a}$	$K_{II}/\tau\sqrt{\pi a}$	Mode I	Mode II	$K_I/\sigma\sqrt{\pi a}$	$K_{II}/\sigma\sqrt{\pi a}$
−90°	8.866	1.037	8.835	1.030	−0.35	−0.65	2.960	0.000
−80°	9.721	0.341	9.793	0.302	0.75	−11.51	2.994	−0.193
−70°	10.871	−0.547	10.862	−0.493	−0.09	−9.80	3.100	−0.405
−60°	11.269	−1.234	11.231	−1.280	−0.33	3.72	3.209	−0.626
−50°	11.145	−1.899	11.213	−2.014	0.61	6.04	3.260	−0.834
−40°	10.871	−2.444	10.905	−2.473	0.32	1.19	3.227	−0.974
−30°	10.237	−2.336	10.348	−2.472	1.08	5.84	3.115	−0.988
−20°	9.621	−1.926	9.669	−1.888	0.50	−1.98	2.961	−0.842
−10°	8.992	−0.501	9.061	−0.591	0.77	17.91	2.825	−0.512
0°	8.695	1.358	8.801	1.339	1.22	−1.42	2.777	0.000
10°	8.857	3.171	8.928	3.294	0.80	3.89	2.825	0.512
20°	9.343	4.646	9.365	4.548	0.24	−2.11	2.961	0.842
30°	9.763	4.966	9.833	5.012	0.72	0.93	3.115	0.988
40°	10.008	4.778	10.082	4.820	0.74	0.89	3.227	0.974
50°	9.862	4.101	9.952	4.150	0.91	1.19	3.260	0.834
60°	9.639	3.410	9.622	3.395	−0.17	−0.45	3.209	0.626
70°	9.218	2.707	9.215	2.647	−0.03	−2.23	3.100	0.405
80°	8.669	1.775	8.722	1.788	0.61	0.74	2.994	0.193
90°	8.866	1.037	8.835	1.030	−0.35	−0.65	2.960	0.000

6.1.1. An inclined crack in rectangular plate under tension

An example of a rectangular plate with an inclined crack under tension is studied. As shown in Fig. 12, the crack is centrally placed at 45°. The crack length to width ratio is selected to be $a/w = 0.2$ and the height to width ratio ranges from 1.0 to 3.0. The material considered is a kind of glass–epoxy composite which possesses the following properties:

$$E_1 = 7.0 \times 10^6 \text{ psi } (48.26 \text{ GPa}), \quad E_2 = 2.5 \times 10^6 \text{ psi } (17.24 \text{ GPa}),$$

$$G_{12} = 1.0 \times 10^6 \text{ psi } (6.89 \text{ GPa}), \quad v_{12} = 0.29.$$

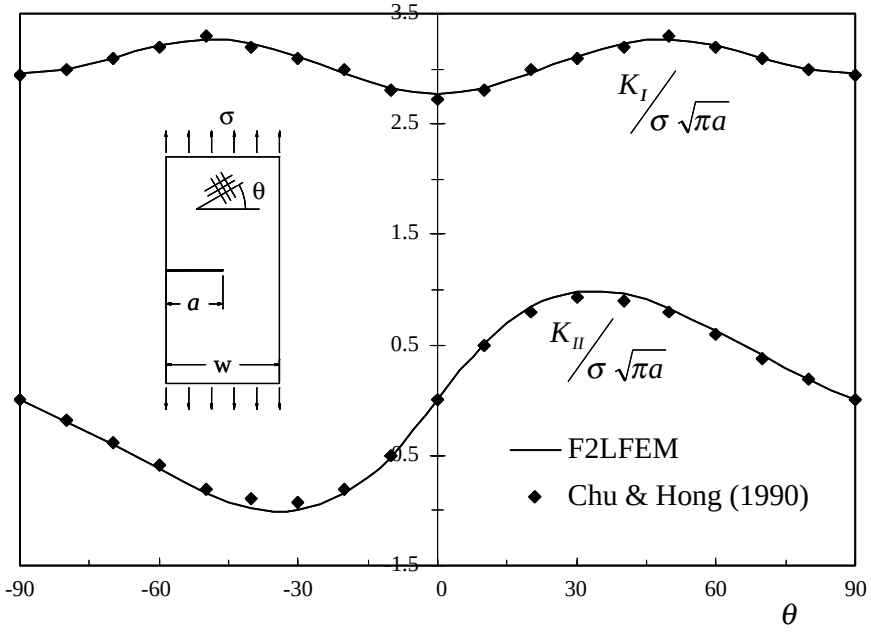

Fig. 11. Variation of $K_I/\sigma\sqrt{\pi a}$ and $K_{II}/\sigma\sqrt{\pi a}$ with material orientation angle θ for single edge cracked plate under tension (material 2).

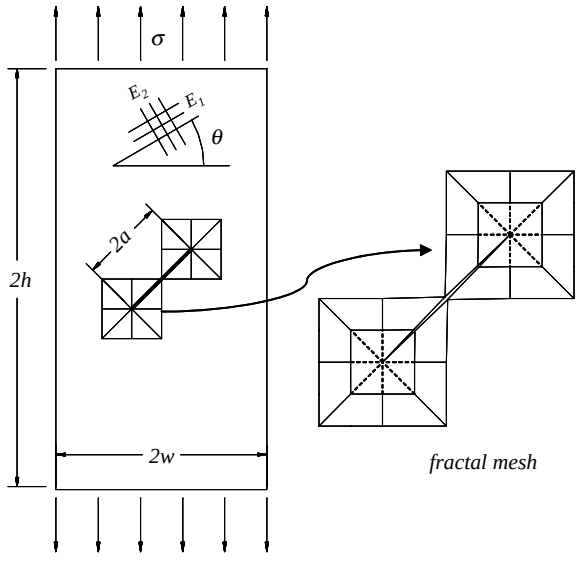

Fig. 12. Inclined crack geometry and fractal mesh configuration.

The dimensionless SIFs $K_I/\sigma\sqrt{\pi a}$ and $K_{II}/\sigma\sqrt{\pi a}$ are calculated in terms of different orientation of material axes θ. The results from F2LFEM and from Gandhi (1972) are tabulated together in Tables 13–15 for $h/w = 1.0$, 2.0 and 3.0 respectively. The errors are found to be less than 1.0% for both modes I and II SIFs.

Table 13
SIFs for inclined crack with rotating material axes θ, $h/w = 1.0$

θ	$K_I/\sigma\sqrt{\pi a}$			$K_{II}/\sigma\sqrt{\pi a}$		
	Gandhi (1972)	F2LFEM	Error (%)	Gandhi (1972)	F2LFEM	Error (%)
0°	0.525	0.5251	0.03	0.516	0.5151	−0.17
45°	0.519	0.5191	0.01	0.514	0.5157	0.34
90°	0.535	0.5395	0.85	0.529	0.5323	0.62
105°	0.543	0.5456	0.47	0.531	0.5357	0.88
120°	0.544	0.5400	−0.73	0.527	0.5286	0.31
135°	0.538	0.5371	−0.17	0.522	0.5236	0.30
180°	0.525	0.5251	0.03	0.516	0.5151	−0.17

Table 14
SIFs for inclined crack with rotating material axes θ, $h/w = 2.0$

θ	$K_I/\sigma\sqrt{\pi a}$			$K_{II}/\sigma\sqrt{\pi a}$		
	Gandhi (1972)	F2LFEM	Error (%)	Gandhi (1972)	F2LFEM	Error (%)
0°	0.522	0.5229	0.17	0.507	0.5066	−0.08
45°	0.515	0.5148	−0.03	0.505	0.5068	0.36
90°	0.513	0.5171	0.81	0.509	0.5117	0.53
105°	0.517	0.5187	0.32	0.510	0.5154	1.06
120°	0.524	0.5201	−0.74	0.512	0.5130	0.20
135°	0.532	0.5306	−0.26	0.511	0.5123	0.26
180°	0.522	0.5229	0.17	0.507	0.5066	−0.08

Table 15
SIFs for inclined crack with rotating material axes θ, $h/w = 3.0$

θ	$K_I/\sigma\sqrt{\pi a}$			$K_{II}/\sigma\sqrt{\pi a}$		
	Gandhi (1972)	F2LFEM	Error (%)	Gandhi (1972)	F2LFEM	Error (%)
0°	0.523	0.5229	−0.02	0.507	0.5064	−0.12
45°	0.515	0.5148	−0.03	0.505	0.5068	0.36
90°	0.512	0.5157	0.73	0.506	0.5092	0.63
105°	0.516	0.5180	0.40	0.509	0.5139	0.96
120°	0.524	0.5202	−0.73	0.511	0.5128	0.36
135°	0.531	0.5306	−0.07	0.511	0.5123	0.25
180°	0.523	0.5229	−0.02	0.507	0.5064	−0.12

7. Conclusions

The extension of F2LFEM to various kinds of anisotropic crack problems has been presented. In this paper, the infinite number of nodal displacements in the singular region is transformed to a new set of generalized coefficients by means of fractal transformation technique. By taking advantage of the dimensional independence of the stiffness matrices of the two-dimensional (2D) elements with similar shape, a single transformation of the stiffness for the first two layers of mesh is enough for all. The number of unknowns is reduced remarkably, and hence the computational effort is substantially decreased. The SIFs can be directly evaluated from the coefficients of global interpolation function. Excellent agreement with error generally less than 1.0% for all four cases of anisotropic crack problems has been obtained.

Acknowledgement

The work described in this paper was fully supported by the grant from the Research Grants Council of the Hong Kong Special Administrative Region, China (project nos. HKU 7014/00E).

References

Bowie, O.L., Freese, C.E., 1972. Central crack in plane orthotropic rectangular sheet. International Journal of Fracture Mechanics 8 (1), 49–57.

Carpinteri, A., Chiaia, B., Cornetti, P., 2001. Static-kinematic duality and the principle of virtual work in the mechanics of fractal media. Computer Methods in Applied Mechanics and Engineering 191 (1–2), 3–19.

Chu, S.J., Hong, C.S., 1990. Application of the J_k integral to mixed mode crack problems for anisotropic composite laminates. Engineering Fracture Mechanics 35 (6), 1093–1103.

Delale, F., Erdogan, F., 1977. The problem of internal and edge cracks in an orthotropic strip. Journal of Applied Mechanics—Transactions of the ASME 44 (2), 237–242.

Gandhi, K.R., 1972. Analysis of an inclined crack centrally placed in an orthotropic rectangular plate. Journal of Strain Analysis 7 (3), 157–162.

Hu, C.B., Li, Y.T., Gong, J., 1998. The transition method of geometrically similar element for dynamic crack problem. Key Engineering Materials 145–149 (Part 1), 267–272.

Kaya, A.C., Erdogan, F., 1980. Stress intensity factors and COD in an orthotropic strip. International Journal of Fracture 16 (2), 171–190.

Lekhnitskii, S.G., 1963. Theory of Elasticity of an Anisotropic Elastic Body. Holden-Day Inc, San Francisco. P. Fern, Trans.

Lekhnitskii, S.G., Tsai, S.W., Cheron, T., 1968. Anisotropic Plates. Gordon and Breach Science Publishers.

Leung, A.Y.T., Su, R.K.L., 1994. Mode I crack problems by fractal two-level finite element methods. Engineering Fracture Mechanics 48 (6), 847–856.

Leung, A.Y.T., Su, R.K.L., 1995a. Body-force linear elastic stress intensity factor calculation using fractal two-level finite element method. Engineering Fracture Mechanics 51 (6), 879–888.

Leung, A.Y.T., Su, R.K.L., 1995b. Mixed mode two-dimensional crack problems by fractal two-level finite element method. Engineering Fracture Mechanics 51 (6), 889–895.

Leung, A.Y.T., Su, R.K.L., 1995c. A numerical study of singular stress field of 3-D cracks. Finite Elements in Analysis and Design 18, 389–401.

Leung, A.Y.T., Su, R.K.L., 1996a. Analytical solution for mode I crack orthogonal to free surface. International Journal of Fracture 76, 79–95.

Leung, A.Y.T., Su, R.K.L., 1996b. Fractal two-level finite element method for cracked Kirchhoff's plates using DKT elements. Engineering Fracture Mechanics 54 (5), 703–711.

Leung, A.Y.T., Su, R.K.L., 1996c. Applications of fractal two-level finite element method for 2D cracks. Microcomputers in Civil Engineering 11 (4), 249–257.

Leung, A.Y.T., Su, R.K.L., 1996d. Fractal two-level finite element analysis of cracked Reissner's plate. Thin Walled Structures 24 (4), 315–334.

Leung, A.Y.T., Su, R.K.L., 1998a. Fractal two-level finite element method for free vibration of cracked beams. Journal of Shock and Vibration 5 (1), 61–68.

Leung, A.Y.T., Su, R.K.L., 1998b. Eigenfunction expansion for penny-shaped and circumferential cracks. International Journal of Fracture 89 (3), 205–222.

Leung, A.Y.T., Su, R.K.L., 1998c. Two-level finite element study of axisymmetric cracks. International Journal of Fracture 89 (2), 193–203.

Panagiotopoulos, P.D., 1992. Fractal geometry in solids and structures. International Journal of Solids and Structures 29 (17), 2159–2175.

Panagiotopoulos, P.D., Panagouli, O.K., Mistakidis, E.S., 1993. Fractal geometry and fractal material behavior in Solids and Structures. Archive of Applied Mechanics 63 (1), 1–24.

Song, C.M., Wolf, J.P., 2002. Semi-analytical representation of stress singularities as occurring in cracks in anisotropic multi-materials with the scaled boundary finite-element method. Computers & Structures 80, 183–197.

Su, R.K.L., Leung, A.Y.T., 2001a. Mixed mode cracks in Reissner plates. International Journal of Fracture 107 (3), 235–257.

Su, R.K.L., Leung, A.Y.T., 2001b. Three-dimensional mixed mode analysis of a cracked body by fractal finite element method. International Journal of Fracture 110 (1), 1–20.

Su, R.K.L., Sun, H.Y., 2002. Numerical solution of cracked thin plates subjected to bending, twisting and shear loads. International Journal of Fracture 117 (4), 323–335.

Su, R.K.L., Sun, H.Y., Leung, A.Y.T., 2003. Determination of crack tip asymptotic stress field by fractal finite element method, Second M.I.T. Conference on Computational Fluid and Solid Mechanics, June 17–20, 2003 at the Massachusetts Institute of Technology, Cambridge, U.S.A. (Accepted).

Su, R.K.L., Leung, A.Y.T., Wong, S.C., 1998. Vibration of cracked Kirchhoff's plates. Key Engineering Materials 145–149, 267–272.

Sun, H.Y., 2003. Fractal Finite Element Method for Anisotropic Crack Problems, M.Phil. thesis, The University of Hong Kong, p. 110.

Tan, C.L., Gao, Y.L., 1992. Boundary element analysis of plane anisotropic bodies with stress concentrations and cracks. Composite & Structures 20, 17–28.